Clay Minerals, (2016) **51**, 793–813

Palaeoclimatic implications of high-resolution clay mineral assemblages preceding and across the onset of the Palaeocene–Eocene Thermal Maximum, North Sea Basin

SIMON J. KEMP[1,*], MICHAEL A. ELLIS[1], IAN MOUNTENEY[1] AND SEV KENDER[1,2]

[1] *British Geological Survey, Environmental Science Centre, Nicker Hill, Keyworth, Nottingham NG12 5GG, UK*
[2] *Centre for Environmental Geochemistry, School of Geography, University of Nottingham, University Park, Nottingham NG7 2RD, UK*

ABSTRACT: Understanding the composition of clay-rich sediments and their transportation into proximal marine basins allows us to better decipher hydroclimatic changes before and within the Palaeocene–Eocene Thermal Maximum (PETM). Only a limited number of such studies exists from the North Sea Basin, which was proximal to the volcanic activity and early rifting hypothesized to have triggered the PETM. The present study examines core material from well 22/10a-4, UK North Sea, as it exhibits an exceptionally expanded and almost stratigraphically complete fine-grained sedimentary sequence suitable for high-resolution analysis.

Quantitative *Newmod-for-Windows*™-modelled clay mineral assemblages, rather than traditional semi-quantitative estimates, are dominated by smectite-rich, interlayered illite-smectite that probably developed from volcanogenic deposits on continental landmasses. Soil development before the PETM is consistent with the existence of a seasonal tropical climate with a prolonged dry season. A striking rise and fall of kaolinite content within the PETM onset, prior to the principal carbon-isotope excursion, is reported here. This variation is interpreted as a signal of an enhanced hydrologic cycle producing an increase in erosionally derived kaolinite, followed by a dampening of this detrital source as sea-levels rose. Global variations in PETM kaolinite concentrations are consistent with a latitudinal shift in patterns of precipitation in models of global warming.

KEYWORDS: Palaeocene–Eocene Thermal Maximum (PETM), clay minerals, kaolinite, erosion, North Sea, 22/10a-4.

The Palaeocene–Eocene Thermal Maximum (PETM), at ~56 Ma, represents arguably the most rapid and significant global warming event in the Cenozoic era. The warming is associated with a carbon isotope excursion ($\delta^{13}C$, CIE) of at least 5‰ consistent with a massive, 2000–12,000 Gt, exogenic pulse of isotopically light carbon to the atmosphere-ocean system and over a time-scale on the order of 100 ky (Röhl *et al.*, 2007; Murphy *et al.*, 2010). The rates of carbon release during the CIE are comparable to the 9 Gt/y produced by current anthropogenic sources (CO_2.Earth, 2016). Consequently the PETM has undergone intensive study as an analogue, or at least a lesson in Earth system behaviour, for anthropogenic climate change. The PETM carbon release was sufficient to raise surface and deep ocean water temperatures by ~5°C (Zachos *et al.*, 2003; Tripati & Elderfield, 2005), with eustatic sea-level estimated to have risen by 3–5 m,

* E-mail: sjk@bgs.ac.uk
https://doi.org/10.1180/claymin.2016.051.5.08

probably as a result of thermal expansion of seawater (Sluijs *et al.*, 2008).

Extensive evidence of an intensified hydrological cycle during the PETM is provided by highly seasonal rainfall, enhanced river discharge and terrestrial input into the oceans (Bowen *et al.*, 2004; Kelly *et al.*, 2005; Pagani *et al.*, 2006; Schmitz & Pujalte, 2007; Sluijs *et al.*, 2007; McInerney & Wing, 2011). In particular, worldwide oceanic records show increased proportions of the clay mineral, kaolinite (Gibson *et al.*, 1993, 2000; Clechenko *et al.*, 2007). Kaolinite develops from the intense weathering of aluminosilicate minerals and generally provides an indication of a warm, humid climate (Chamley, 1989; White & Brantley, 1995; Thiry, 2000). However, as kaolinite may have taken 1–2 My to form during the peak warmth and CO_2-rich atmospheric conditions of the Cretaceous (Thiry, 2000), some authors have questioned whether its appearance during the PETM signifies concomitant warming and precipitation (*e.g.* Gawenda *et al.*, 1999), but instead points to seasonal erosion of pre-existing deposits during the PETM (*e.g.* Thiry, 2000; Berggren *et al.*, 2012; John *et al.*, 2012). Although these phenomena have been described widely, geographic variability is still poorly understood, even for the circum-North Atlantic region from where several datasets exist (*e.g.* Schmitz & Pujalte, 2003; John *et al.*, 2008, 2012; Dypvik *et al.*, 2011; Kender *et al.*, 2012).

A significant and outstanding question is the relative timing of the major carbon release and an intensified hydrological cycle. This is an important issue because it speaks to the cause of carbon release and to the existence of possible early warning signals of global environmental instability. The rate of sedimentation represented in most PETM cores is insufficient to resolve this relative timing at the time scale on the order of 10^3 y, and so it has been assumed that the release of carbon triggered global warming and the subsequent change in hydrology. Increasing evidence, however, suggests that the onset of environmental change, including an intensified hydrological cycle, occurred prior to the CIE by several thousand years (Sluijs *et al.*, 2007; John *et al.*, 2012; Kender *et al.*, 2012).

Here, the nature of the clay mineralogy across the PETM transition from a cored interval in the central North Sea Basin is reported (22/10a-4; Fig. 1), in particular to examine any hydrologically associated variations during the onset of the PETM. Knox (1996) previously presented low-resolution clay mineral data from 22/10a-4 and his detected increase in kaolinite was later shown to coincide approximately with the onset of the CIE (Kender *et al.*, 2012). Kender *et al.* (2012) also used palynological, geochemical and sedimentological proxies to reveal enhanced halocline stratification and terrigenous deposition well before (10^3 y), at the onset of, and within the earliest CIE. The present study takes advantage of high-resolution sampling of the same core as investigated by Knox (1996) and Kender *et al.* (2012), and improvements to clay mineral quantification, to reconstruct a higher-fidelity record that uncovers the details of its lead/lag relationship with carbon release.

GEOLOGICAL SETTING

The North Sea Basin first developed as an extensional basin through rifting along the axes of the Central, Viking and Witch Ground grabens during the Late Permian/Triassic (Glennie, 1986) (Fig. 1). Further rifting and block faulting occurred during the Late Jurassic and Early Cretaceous with subsidence continuing to the present day. Cretaceous and Tertiary sediments represent the majority of the sedimentary fill. The basin is bounded by the major landmasses of Scotland, the Fenno-Scandian shield and, until the Eocene, Greenland. A marine connection existed periodically to the south but has generally been continually open to the north, to the Boreal Ocean. A restricted, marine depositional environment, characterized by siliciclastic sedimentation and high terrigenous input, has therefore prevailed with the exception of delta progradation in the Middle Jurassic and locally during the Late Jurassic and Palaeocene (Pearson, 1990; Knox, 1998).

The provenance of the sediment, including clay minerals, supplied to the North Sea Basin has varied over time as tectonics have exposed different land areas and drainage patterns have changed. Initially, the granitic and metamorphic terrains of Scandinavia and northern Scotland together with the Devonian sedimentary rocks of the East Shetland Platform are likely to have made substantial contributions (Pearson, 1990). Northward supply is more uncertain and variable with Devonian and Carboniferous sources through much of the Jurassic and Cretaceous (Ziegler, 1982) and erosion of basic Forties volcanics in the Middle Jurassic. However, during the early Tertiary, airfall volcanic ash probably covered land areas to a large extent and is likely to have dominated erosion products (Pearson, 1990). Sediment movement southwards into the northern North Sea Basin from Greenland was probably impeded by the Faeroe–Shetland Trough which may have existed since the Carboniferous (Haszeldine & Russell, 1987), though fine detritus may have been unobstructed.

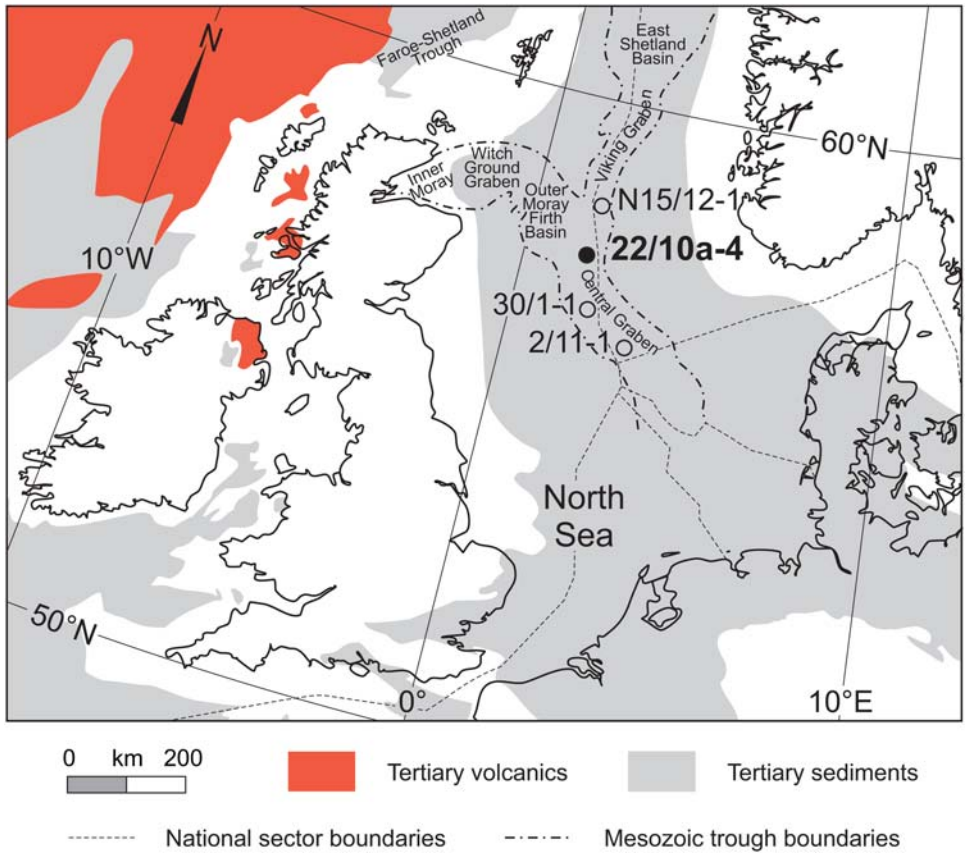

FIG. 1. Map showing the location of North Sea study site well 22/10a-4 and other sites described in this study in relation to the main Mesozoic structural elements and distribution of Tertiary sediments and volcanics (modified from several maps from King, 2016).

Well 22/10a-4 is situated in the central part of the North Sea Basin (Fig. 1), distant from land masses and marginal-marine processes (*e.g.* river, wave, current or tidal effects) that could disguise oceanographic indicators (Kender *et al.*, 2012). Palaeo-ecological micropalaeontology methods (Gillmore *et al.*, 2001) combined with 2D structural restoration (Kjennerud & Sylta, 2001) suggest that the central parts of the northern North Sea have experienced palaeodepths of >0.5 km during the earliest Eocene (Kjennerud & Gillmore, 2003). Owing to its depocentre location, the core obtained from 22/10a-4 exhibits an exceptionally expanded and almost stratigraphically complete Palaeocene–Eocene transition sequence. Minor erosion at the base of thin turbidite sandstones (typically <10 cm) provides the only evidence for breaks in the succession (Kender *et al.*, 2012). A lack of diagenetic alteration suggests that the sequence has only undergone shallow burial (*e.g.* Nielsen *et al.*, 2015).

Late Palaeocene regional uplift, associated with the proto-Iceland mantle plume in the North Atlantic (Knox, 1996), led to a sea-level fall of the order of 100 m and the basin becoming more restricted. This drop in sea level produced a lithological change from pale greyish green, waxy bioturbated claystones to medium to dark-grey laminated mudstone and demarcation of the boundary between the lower Lista and upper Sele formations (Figs 2 and 3). Basin restriction also stagnated bottom waters, and led to a change in the benthic foraminiferal assemblages to low-diversity, low-oxygen-tolerant agglutinated species (Knox, 1996; Kender *et al.*, 2012).

Relative sea-level rise within the early PETM has been inferred from sections in the Atlantic, Pacific,

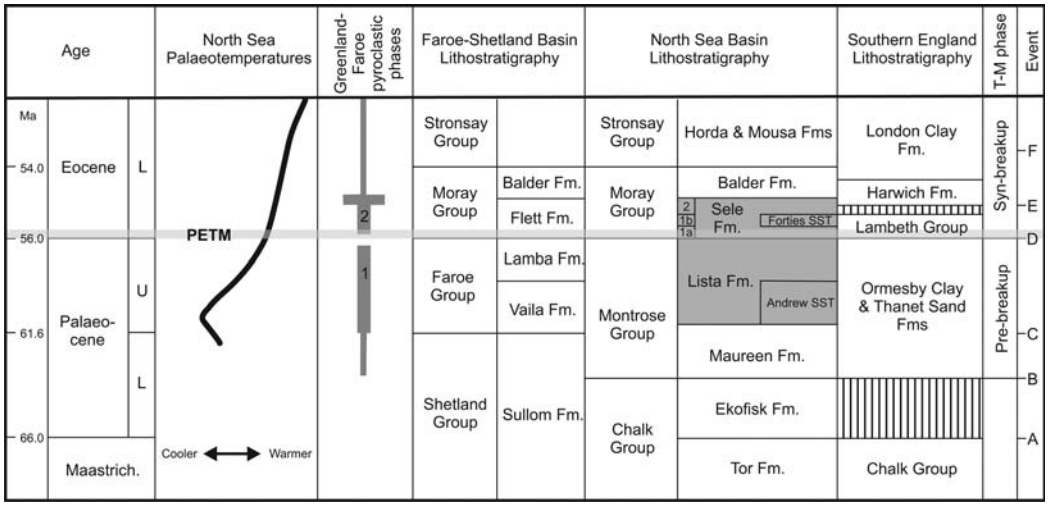

FIG. 2. Palaeocene–Lower Eocene stratigraphy of the North Sea and Faroe-Shetland basins compared to southern England (modified from Huggett & Knox, 2006; Mudge, 2015). Pyroclastic phases 1 and 2 from Knox & Morton (1988). T-M = tectonic-magmatic phase. Tectonic events: A = short-lived regional uplift; B = regional plume-induced uplift; C = uplift of Scottish source areas; D = regional uplift (N. Atlantic thermal updoming); E = onset of NE Atlantic sea-floor spreading and regional thermal subsidence; F = regional uplift.

Tethyan and Arctic oceans and the Turgay Strait (Harding *et al.*, 2011). However, clay mineral assemblage and oxygen-isotope records from the New Jersey margin (John *et al.*, 2012) suggests that the onset preceded the PETM by 20–200 ky, and is supported by further data from Spitsbergen (Harding *et al.*, 2011). Sluijs *et al.* (2008) suggested the thermal expansion of seawater, melting from small-scale Antarctic alpine glaciers and/or a decrease in ocean-basin volume (caused by tectonics/volcanism associated with the North Atlantic Igneous Province, NAIP) as possible mechanisms for the pre-CIE sea-level rise.

Previous North Sea Tertiary clay mineral studies

Despite the wide extent and substantial thickness (up to 3500 m) of the UK offshore Tertiary succession, published clay mineralogical data for these sedimentary rocks are limited (Huggett & Knox, 2006) but have recently been augmented by a further review of the Norwegian and Danish sectors (Nielsen *et al.*, 2015).

Pearson & Small (1988) and Pearson (1990) analysed shale cuttings from six wells from the East Shetland Basin, Viking Graben, Inner and Outer Moray Firth Basin, to the north and northwest of the present study area. They found that the Palaeocene to Eocene succession is composed predominantly of smectite-rich R0-ordered interlayered illite-smectite (I-S) with minor illite, kaolinite and variable amounts of chlorite. However, they failed to distinguish between kaolinite and chlorite in many of the studied wells.

Similarly, in the very southwest of the Norwegian sector and south-east of 22/10a-4, the clay mineralogy of Palaeocene shales in well 2/11-1 (Fig. 1) is dominated by smectite with only minor amounts of kaolinite and illite (Karlsson *et al.*, 1979). Eocene shales show a gradual upwards increase in illite and kaolinite (Karlsson *et al.*, 1979). Elsewhere in the Norwegian sector, the Palaeocene and lower Eocene sedimentary rocks in well N15/12-1 are also dominated by smectite with only minor amounts of illite, kaolinite and chlorite, the latter being distinctly Fe-rich (Berstad & Dypvik, 1982). Clay assemblages in well 30/1-1 (Fig. 1), to the south of the present study area, exhibit similar trends to those described for the Norwegian sector. Large smectite contents have also been observed in Tertiary mudrocks from onshore Denmark (Nielsen, 1974).

The low-resolution study of Knox (1996) was the first to note the kaolinite-free nature of the clay mineral assemblages in the Lista Formation, which are dominated by smectite or chlorite and initially persist into the lower part (Unit 1a) of the Sele Formation in 22/10a-4 (Fig. 3). Kaolinite appears about half way up Unit 1a, reaching a low peak within a turbidite sandstone unit. After a slight decrease in the lower

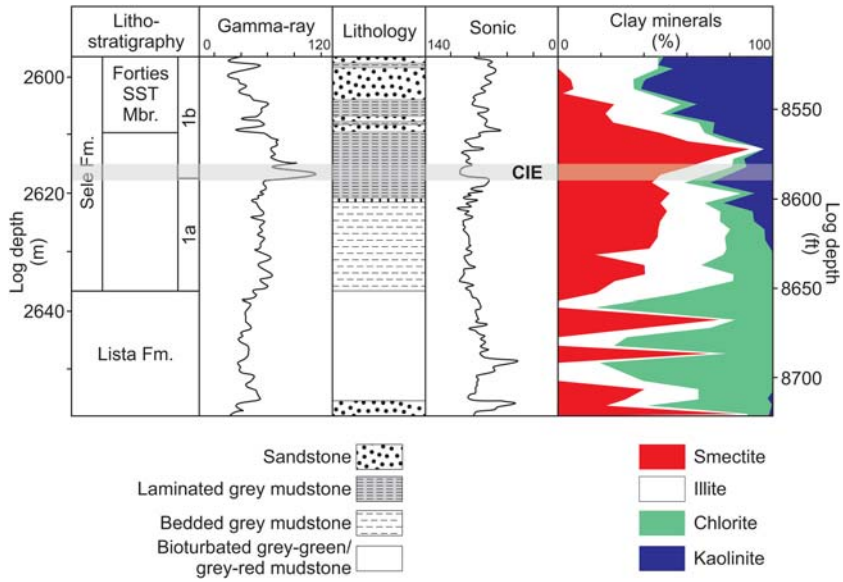

FIG. 3. Lithological, gamma-ray and sonic wireline geophysical logs and low-resolution sediment core clay mineralogy for well 22/10a-4 plotted against logging depth (modified from Knox, 1996; Huggett & Knox, 2006). Huggett & Knox (2006) later identified the Sele Formation 1a/1b unit boundary at 2609.5 m (core depth). Kender *et al.* (2012) identified the carbon isotope excursion (CIE) of the PETM, and raised the Lista/Sele formation boundary to 2630.5 m (core depth). With the exception of this figure, all sample depths used in this study are core depths.

part of Unit lb, kaolinite increases rapidly, paralleling an overall increase in grain size.

MATERIALS AND METHODS

Core samples from the Sele and Lista formations from well 22/10a-4 (57°44′8.47″N; 1°50′26.59″E) consist of variably fissile claystone with interbedded fine- to coarse-grained sandstone layers interpreted as turbidites, with occasional mm-thick ash layers (Fig. 3). In total, 100 samples were collected for clay mineralogical X-ray diffraction (XRD) analysis from claystone horizons only, avoiding sandstone beds. The section of 22/10a-4 analysed in this study is from 2596.5 to 2651.6 m (core depth), chosen because this part of the core is predominantly in claystone facies and provides a greatly expanded section over the onset of the CIE (Fig. 3). Between core depths of 2609 and 2613 m the claystone becomes finely laminated with alternately pale and dark laminae couplets ranging from 1 to 25 per mm. The pale laminae consist of clay and silt, and the dark laminae are rich in organic carbon and pyrite inclusions (Kender *et al.*, 2012).

There is some debate about the placement of the boundaries between the Lista and Sele formations and the subdivision of the Sele Formation into units 1a and 1b. On the basis of geophysical log response, Knox (1996) placed the former at 2636.5 m and the latter at 2617.5 m (Fig. 3). In a later paper (Huggett & Knox, 2006), the Sele Unit 1a-1b boundary was moved higher to beneath the lowermost sandstone at 2609.5 m, presumably using core-depth data. Kender *et al.* (2012) placed the core boundary between the Lista and Sele formations at 2630.5 m, proposing a −6 m offset between log and core depths. Excluding Fig. 3 which shows geophysical log depth, core depths including the Lista-Sele formation boundary (2630.5 m) and Sele Unit 1a-1b boundary (2609.5 m) have been used throughout this study.

The XRD methodology employed here broadly follows that used in two previous PETM clay mineral studies (Harrington & Kemp, 2001; Harrington *et al.*, 2004). However, in order to initially compare results with those obtained previously from well 22/10a-4 (Knox, 1996), a nominal <4 μm size fraction was isolated and analysed, rather than the more traditional <2 μm size fraction employed in most studies. On sedimentological grounds, <4 μm reflects clay-grade particles (Wentworth, 1922). Because smectite is typically composed of finer-grained particles than other clay minerals (Moore & Reynolds, 1997), the finer the fraction isolated, the greater

the proportion of smectite that will be recorded. Therefore, where smectite is common, analysis of the <4 μm fractions enables more sensitive monitoring of changes in the clay mineral assemblage composition. For this study, the desire for such sensitive monitoring outweighed the requirement to compare directly with previous <2 μm fraction regional data.

Sample preparation

In order to reduce the proportion of non-clay minerals present in isolated fine-size fractions for clay mineral XRD analysis, these should ideally be prepared from crushed (not milled) material. We therefore targeted crushed material, apart from when only milled material was available (24 samples). Approximately similar particle-size and XRD results from juxtaposed milled and crushed materials suggest that, in this case, the different sample forms do not appear to have adversely affected the analytical results produced.

A representative ~4 g portion of each core sample was removed and crushed in a pestle and mortar to pass a 2 mm sieve. The <2 mm (or in some cases milled) material was then dispersed in deionized water using a reciprocal shaker combined with treatment with ultrasound. The resulting suspensions were then sieved on a 63 μm aperture sieve and the >63 μm ('sand') material was dried at 55°C and bagged. The <63 μm material was placed in a 250 mL measuring cylinder with a few drops of 0.1 M sodium hexametaphosphate ('Calgon') solution to disperse the individual clay particles and prevent flocculation.

After standing for a period determined by Stokes' Law, a nominal <4 μm fraction was removed in a single extraction. The <4 μm ('clay') material and remaining 4–63 μm ('silt') material were then dried at 55°C and stored in glass vials.

So that similar amounts of material were mounted and exposed to the X-ray beam, ~100 mg of the <4 μm material was re-suspended in a minimum of deionized water and pipetted onto a ceramic tile in a vacuum apparatus to produce an oriented mount. In order to remove the effects of the 'Calgon' addition and/or possible seawater interaction, homionic Ca-saturated mounts were produced by adding 2 mL of 0.1 M $CaCl_2.6H_2O$ solution, washing twice to remove excess reagent before drying at room temperature.

Clay mineral analysis

The XRD analysis was carried out using a PANalytical X'Pert Pro series diffractometer equipped with a cobalt-target tube, X'Celerator detector and operated at 45 kV and 40 mA. The <4 μm oriented mounts were scanned from 2 to 40°2θ at 1.02°2θ/min after air-drying, ethylene glycol-solvation (16 h) and heating at 550°C (2 h). Clay mineral species were then identified from their characteristic peak positions and intensities and their reaction to the diagnostic testing program.

With the exceptions of Harrington & Kemp (2001) and Harrington *et al.* (2004), previous palaeoclimatic and PETM clay mineralogical studies have all employed relatively simple XRD peak area/height measurements and correction multipliers to determine semi-quantitative estimates of the clay minerals present (*e.g.* Pearson & Small, 1988; Pearson, 1990; Harding *et al.*, 2011; John *et al.*, 2012; Bornemann *et al.*, 2014; Hermoso & Pellenard, 2014; Lombardi, 2014). Such semi-quantitative methods (most commonly based on Biscaye, 1965), are objective, reproducible and have been used extensively by sedimentologists to provide fit-for-purpose comparisons of regional datasets.

However, as acknowledged by Biscaye (1965), the intensity of a clay mineral's characteristic XRD peaks cannot be used as a direct measure of its abundance because of variations due to machine conditions, sample-mount thickness, the degree of clay mineral preferred orientation and the variable 'diffractability' of different clay minerals. Critically, the Biscaye (1965) method only provides rough estimates of interlayered clays and takes no account of variations in the crystal order and chemical composition of different species of the same mineral. The latter also mean that pure mineral standards (Huggett, 1992, 1996) have limited use in this regard. Weighted peak-area percentages are constructs and, at best, are untestable approximations of real percentages (Biscaye, 1965) with precision estimated to be >±5 to 10% of the amount present at percentages >15% (Schultz, 1964). For detailed clay mineralogical studies, therefore, a more rigorous methodology producing quantitative data is clearly desirable.

Although quantitative evaluation of clay mineralogy was not achievable in the 1960s (Biscaye, 1965), more recent advances, particularly in the computer modelling of XRD profiles (*e.g. Newmod-for-Windows*™, Reynolds & Reynolds, 1996; *SYBILLA*, Zeelmaekers *et al.*, 2007) have helped to deliver realistic quantitative data (Zeelmaekers *et al.*, 2015).

The modelling-based methodology used in the present study (and previously by Harrington & Kemp, 2001; Harrington *et al.*, 2004) holds several key advantages over the peak area/height techniques. Importantly, modelling allows changes in both the crystal order (crystallite-size

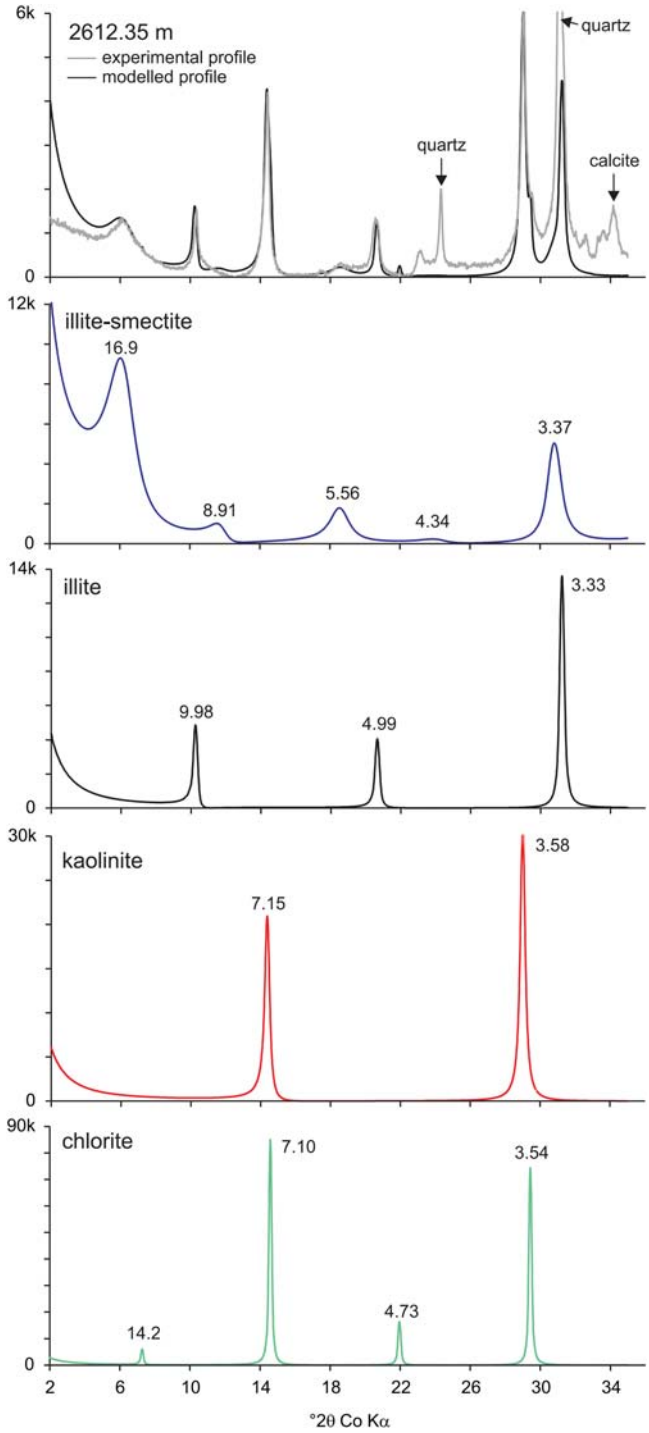

FIG. 4. Comparison of a composite modelled XRD profile with an experimental ethylene glycol-solvated XRD trace; sample depth 2612.35 m, Sele Formation Unit 1a (upper figure). Modelled XRD traces for each clay mineral component (illite-smectite, illite, kaolinite and chlorite) with peak positions (Å) are shown in the lower four figures. Note the different intensity scales for the component traces.

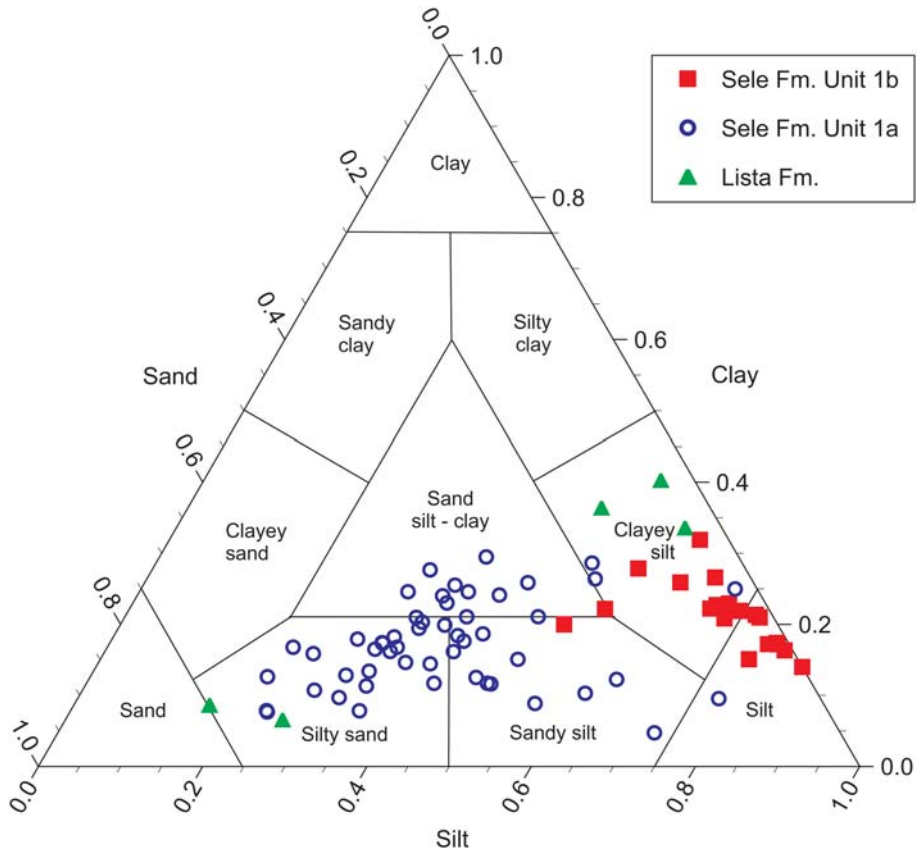

FIG. 5. Triplot particle-size distribution for the 22/10a-4 samples (after Shepard, 1954).

distribution) and chemistry of clay mineral species to be taken into account on a sample-to-sample basis. The pattern fitting/deconvolution approach employed during modelling also facilitates the more accurate interpretation of peak overlaps, a particularly important feature when distinguishing and quantifying kaolinite in the presence of chlorite, critical for this study.

Modelling of the <4 μm glycol-solvated XRD profiles was carried out using *Newmod-for-Windows*™ (Reynolds & Reynolds, 1996) software on all the samples. The modelling process requires the input of diffractometer, scan parameters and a quartz intensity factor (instrumental conditions), and the selection of different sheet compositions and chemistries. In addition, an estimate of the crystallite-size distribution of the species may be determined by comparing peak profiles of calculated diffraction profiles with experimental data. By modelling the individual clay mineral species in this way, 'mineral reference intensities' were established and used for quantitative standardization following the method outlined by Moore & Reynolds (1997).

An example of the excellent fit of a modelled profile with that produced by one of the samples is shown in Fig. 4.

RESULTS

Particle-size distribution

As part of the preparation procedure for XRD analysis, approximate particle-size data were produced (% 'sand', 'silt' and 'clay'). Note, however, that as full recovery of <4 μm material was not achieved, the particle-size data overestimate the 'silt' fraction and underestimate the 'clay' fraction proportions of the samples and should only be regarded as indicative. Our previous experiments suggest that >70% of the <4 μm material present in a typical mudstone sample is removed in a single extraction, >95% after two extractions.

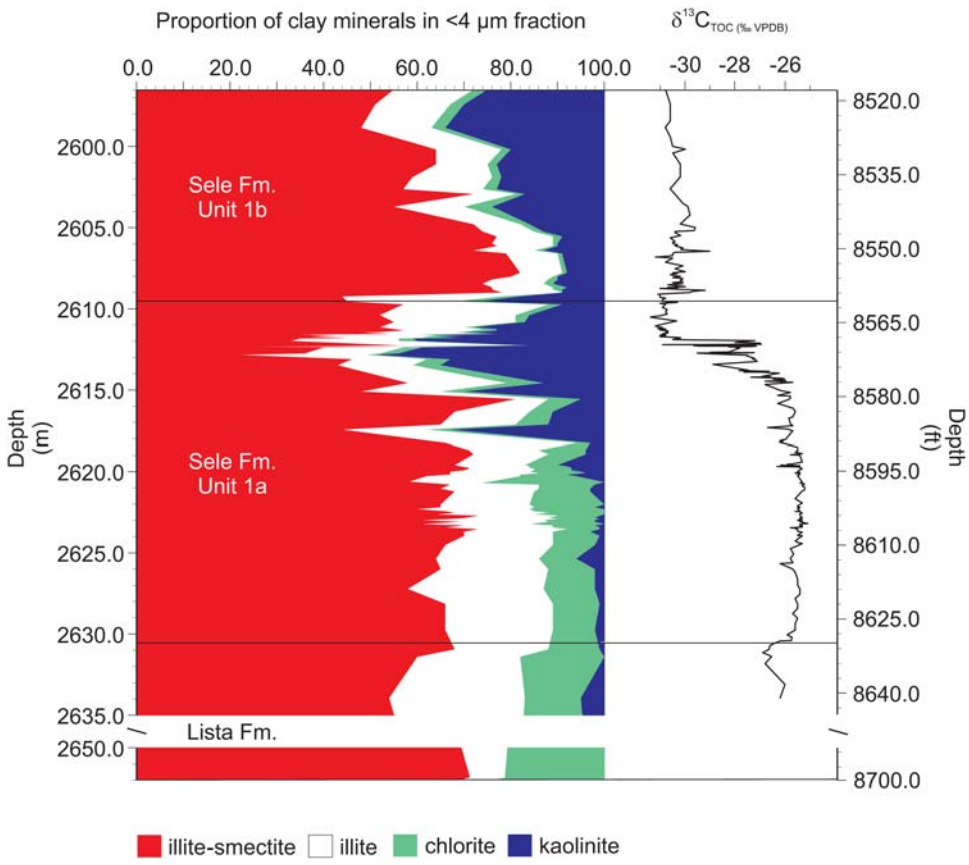

FIG. 6. Downhole distribution of clay minerals for the 22/10a-4 samples as a proportion of the <4 µm fraction, compared to the carbon isotope measurements on total organic carbon (TOC) (from Kender *et al.*, 2012).

The particle-size data show a marked upwards fining through the 22/10a-4 sampled sequence (Fig. 5). Using the classification of Shepard (1954), the two deepest samples from the Lista Formation are relatively coarse-grained sands/silty sands while the shallower samples are much finer, clayey silts. The overlying Sele Formation Unit 1a is also composed predominantly of silty sands/sandy silts/sand silt-clays with occasional clayey silts. In comparison, the Sele Formation Unit 1b is composed of silts, clayey silts and rarely sandy silts.

Berstad & Dypvik (1982) present approximately similar particle-size distributions from the Palaeocene and Eocene sediments of a Norwegian sector well (N15/12-1, Fig. 1) to those found in 22/10a-4. The generally silty clays show an overall fining-up sequence with decreasing sand content similar to the present study.

Clay mineralogy

The XRD analysis revealed that the clay mineral assemblages of the deepest samples from the coarser-grained lithologies of the Lista Formation (below 2650 m), are dominated by an interlayered illite-smectite (I-S, mean 70%) with moderate amounts of chlorite (mean 23%) and minor amounts of illite (mean 7%) (Fig. 6). No kaolinite was detected in these samples (Fig. 7a).

The XRD peak positions for the Ca-saturated mounts together with *Newmod-for-Windows*™-modelling of the glycol-solvated XRD profiles suggests that the I-S is an R0-ordered 40% illite: 60% smectite species, in which the illite layers have a 0.1 Fe, 0.7 K per $(Si, Al)_4O_{10}(OH)_2$ chemistry and which has a crystallite-size distribution with a mean defect-free distance of four layers and a range of 1–15 layers. The lack of kaolinite in these samples enables more accurate characterization

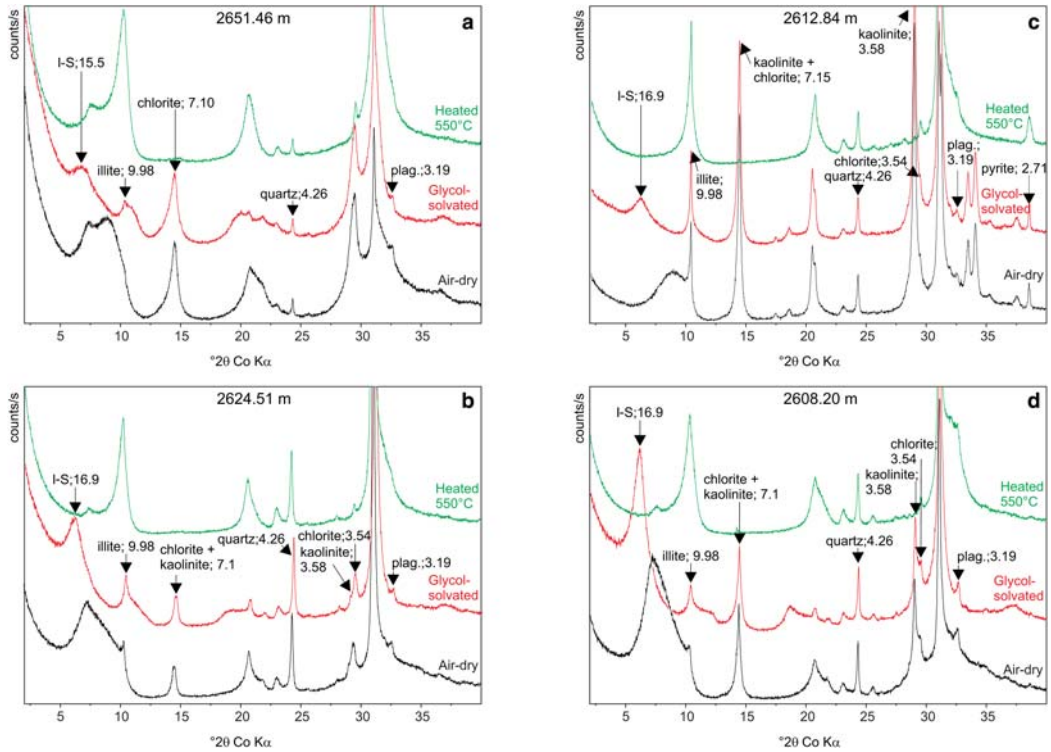

FIG. 7. Sample XRD traces (air-dry, ethylene glycol-solvated and heated 550°C) to illustrate the clay mineral assemblages identified in the 22/10-a4 samples: (a) Lista Formation, 2651.46 m; (b) Sele Formation Unit 1a base and middle, 2624.51 m; (c) Sele Formation Unit 1a upper, 2612.84 m; and (d) Sele Formation Unit 1b, 2608.20 m.

of the chlorite, which is very Fe-rich with a mean defect-free distance of four layers and a crystallite-size range of 1–14 layers. The illite has a composition 0.05 Fe, 0.7 K per $(Si, Al)_4O_{10}(OH)_2$, a crystallite-size range of 1–60 layers and a mean defect-free distance of 19 layers.

The clay mineral assemblages of samples from the upper Lista Formation and the base and middle of the Sele Formation Unit 1a (2635–2620 m) are also dominated by I-S with minor amounts of illite and chlorite together with the appearance of traces of kaolinite (Figs 6 and 7b). The illite and I-S detected in these samples is generally similar to that found in the lower Lista Formation; the I-S again being identified as an R0-ordered 40%I species. *Newmod-for-Windows*™-deconvolved kaolinite d_{001} XRD peak widths (full width at half maximum, FWHM, mean 0.38°2θ), isolated from the chlorite d_{002} input, indicate moderate crystal order with a mean defect-free distance of 15 layers and a crystallite-size distribution range of 1–60, 7 Å layers. The chlorite has a more intermediate Fe/Mg chemistry compared to that identified in the deeper Lista Formation samples.

The upper part of Sele Formation Unit 1a (from 2620 to 2609.5 m) shows clay mineral assemblages with decreasing proportions of I-S, increasing proportions of kaolinite with minor illite and only traces of chlorite (Figs 6 and 7c). Towards the base of this interval the I-S retains a similar R0-ordered 40%I composition but from ~2618 m upwards, the I-S increasingly exhibits a more smectitic character (R0-ordered 30%I). While the illite and chlorite retain similar characteristics to those detected in the base and middle of the Sele Formation Unit 1a, the increased kaolinite exhibits sharper, deconvolved XRD peaks (d_{001} FWHM, mean 0.30°2θ) indicative of a more highly ordered nature. *Newmod-for-Windows*™-modelling suggests that kaolinite crystallite-size distributions reach mean defect-free distances of 40 layers and a range of 1–80, 7 Å layers.

Above 2609.5 m, the clay mineral assemblages of Sele Formation Unit 1b continue to be dominated by I-S. An R0-ordered 30%I species is most prevalent at the base of the interval but considerably more variable and illite-rich species with up to 80%I were detected in the shallowest samples. Minor proportions of kaolinite

and illite were also detected together with traces of chlorite in these samples (Figs 6, 7d). Kaolinite crystal order (d_{001} FWHM, mean 0.33°2θ) and chlorite chemistries generally appear similar to the upper part of Unit 1a.

Clay mineral indices

The PETM studies that include clay mineralogical analyses frequently determine clay mineral ratios (*e.g.* kaolinite/smectite, K/S and kaolinite/illite, K/I) in order to provide indices for estimating environmental change (*e.g.* Robert & Kennett, 1994; Bolle & Adatte, 2001; John *et al.*, 2012). Chamley (1989) advocates the use of relative variations in the abundance of different clay minerals rather than absolute values in palaeoclimatic reconstructions, in order to differentiate their erosion from soil or rocky substrates. However, different authors have determined these apparently similar ratios in different ways. Bolle & Adatte (2001) calculated their K/S index using a ratio of ethylene glycol-solvated XRD peaks (kaolinite ~7.1 Å and smectite ~16.9 Å); although they provide no indication of whether peak heights or areas were measured. Robert & Kennett (1994) used peak-height data for the same peaks. More recently, John *et al.* (2012) measured XRD background-subtracted peak heights adjusted by form-factors for the different clay minerals. Comparison of these semi-quantitative values and ratios with the more accurate, quantitative clay-mineral data and ratios that can now be routinely produced, are clearly restricted to trend commentaries.

We also present clay mineral indices for kaolinite/(illite-smectite) (K/(I-S)) and K/I to aid comparison with previous studies. However, rather than simply ratioing peak-area measurements (raw or adjusted) from XRD traces, the present indices were calculated from modelled clay mineral proportions and therefore more accurately reflect actual clay mineral variation.

Both K/(I-S) and K/I values are consistently low and close to zero through the Lista Formation and older part of the Sele Formation Unit 1a (below ~2620 m, Fig. 8). Both indices show single-point peaks (~2617 and ~2615 m) prior to complex multi-peaked maxima at ~2612–2613 m), after which they fall to background levels during the bulk of the CIE excursion (*i.e.* above 2611.5 m). Importantly, the rise and fall of the clay indices occurs prior to the principal CIE (*i.e.* carbon release). The transition from Sele Formation Unit 1a to 1b is marked by further, minor K/(I-S) and K/I spikes. Decreasing depth within the Sele Formation Unit 1b is characterized by a gradual overall K/(I-S) increase together with a much more pronounced increase in K/I (Fig. 8) reflecting a reduction in the relative proportion of illite in the youngest rocks (Fig. 6).

DISCUSSION

This study indicates the predominance of smectite-rich I-S in the PETM sequence of 22/10a-4 and differs from many previous North Sea studies where discrete smectite has been described. These include that by Knox (1996) who examined the same core interval, albeit at a much lower resolution and included coarser-grained lithologies. Sedimentologists have frequently used the term 'smectite' to include smectite-rich I-S (*e.g.* Chenot *et al.*, 2016) but in most cases, including Knox (1996), this simplification is not detailed and therefore ambiguous. The XRD responses of discrete smectite and smectite-rich I-S are similar in terms of peak position behaviour, and speciation can be difficult where assemblages are complex and severe peak-overlap issues occur in the diagnostic low-angle region. However, the current authors contend that accurate speciation, significantly aided by modelling approaches, is critical. *Newmod-for-Windows*™ modelling suggests that peak areas for the lowest-angle basal spacing, the sole basis for traditional semi-quantitative estimates, can vary dramatically between discrete smectite and smectite-rich I-S and therefore yield very different concentrations and clay mineral indices. Comparison of data produced from semi-quantitative peak areas (Knox, 1996) and *Newmod-for-Windows*™ modelling concentrations (this study) in Figs 3 and 6 indicates that Knox (1996) substantially underestimated the proportion of smectite-rich I-S present in the sequence.

Further comparison between the two datasets highlights that the *Newmod-for-Windows*™-modelling approach is more successful in detecting kaolinite in the presence of chlorite (Figs 3 and 6).

Clay mineral provenance

The highly smectitic nature of the Tertiary sedimentary sequence in the North Sea (and onshore in Denmark) is considered to be the end-result of episodes of explosive volcanic activity (*e.g.* Malm *et al.*, 1984; Pearson, 1990; Nielsen *et al.*, 2015). Petrographic and mineralogical identification of glass, plagioclase, anatase, zeolites and carbonates provide further evidence for a significant volcaniclastic component in these sediments (*e.g.* Karlsson *et al.*, 1979; Huggett, 1992).

Volcanic material was available from two phases of volcanic activity associated with the opening of the NE

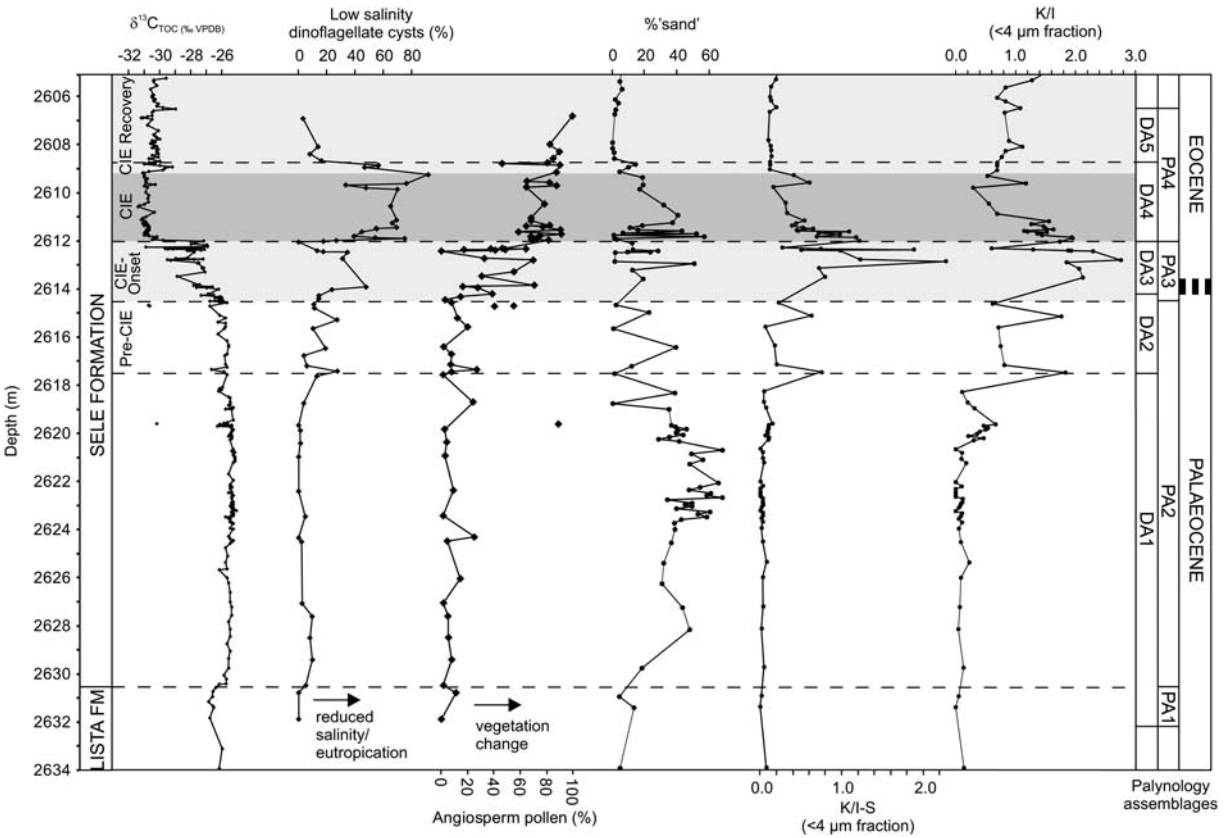

FIG. 8. Downhole variation in clay mineral indices for the 22/10a-4 samples: K/(I-S) and K-I and %'sand' compared to total organic carbon (TOC) isotopic and micropalaeontological proxies from the same core (from Kender *et al.*, 2012). The carbon isotope excursion (CIE) can be correlated to the global CIE of the PETM.

Atlantic and with the Faeroe–Shetland rift (Fig. 2). Firstly, 1–3 m thick tholeiitic basalt ash beds (Knox & Morton, 1988) are interbedded with mudrocks in lower Palaeocene deposits in the northeastern Atlantic region (Huggett, 1992). Secondly, >200 ashfalls have been recorded from more acidic volcanoes in Early to Mid-Eocene deposits in the Faroes–Greenland area (Huggett, 1992). On the basis of uranium, thorium and potassium geochemistry, Berstad & Dypvik (1982) estimated that Palaeocene and lower Eocene sediments in well N15/12-1 have a 60–80% pyroclastic origin. Post-Mid-Eocene sediments have greater concentrations of these elements and produce an increased gamma-ray response reflecting a decreasing pyroclastic (~20%) and increased terrestrial input (Berstad & Dypvik, 1982). However, there is debate about whether volcanic material was initially deposited in the North Sea, on adjacent landmasses, or in both locations (Nielsen *et al.*, 2015).

Marine development. Early workers favoured an *in situ* development of smectite *via* the halmyrolitic alteration of volcanic glass and ash (*e.g.* Karlsson *et al.*, 1979). Volcanism was further evidenced by the presence of sponge spicules and radiolarian tests representing organism blooms, stimulated by high-silica brines (Berstad & Dypvik, 1982). We note that smectite and I-S may also develop by direct precipitation from the mixing of marine waters and hydrothermal fluids on the sea floor (*e.g.* Alt & Jiang, 1991; Inoue, 1995). Previous workers have discounted this mechanism, presumably due to the large geographical extent of the smectite in the Tertiary sediments and the lack of other hydrothermal influences (Huggett & Knox, 2006).

Nielsen *et al.* (2015) suggest that differences they noted in smectite interlayer cations indicate different development paths. Monovalent (Na^{+}) types reflecting direct formation from volcanic ash in the depositional environment while divalent (Ca^{2+}) types infer smectite supplied from surrounding land areas. However, such differences in XRD peak positions may again reflect the mis-identification of I-S or alternatively the differential interaction of smectite with seawater/soluble salts. The clay mineral assemblages in the present study were dispersed using 'Calgon' and subsequently saturated with Ca^{2+} and their *in situ* interlayer cation chemistry therefore cannot be identified.

Continental development. Continental authigenesis of precursor smectite is limited to two possible environments: relatively common soil development, or rarer precipitation in saline, alkaline lakes. On the basis of its rarity and a lack of lacustrine facies, the latter environment is discounted in this case.

Widespread soil authigenesis of smectite-group clay minerals is typically associated with vertisols, formed in seasonal tropical climates with a dry season of 4–8 months, such as that found in present day India, eastern Australia, Sudan, Ethiopia, Kenya, Chad and the lower Parana River in South America (Chamley, 1989; Righi & Meunier, 1995; Bergaya *et al.*, 2006). On Fe-Mg-rich parent rocks such as basalt or volcanic ash, leaching of cations (Ca, Mg) is minimized and with favourable high pH, smectite develops. Vertisols typically exhibit wide and deep cracks due to seasonally-induced, alternate shrinking and swelling. Such processes cause self-mulching and the development of an extremely deep A horizon (the surface mineral soil) and no B horizon (subsoil).

It is likely that sufficient volumes of volcanic products were deposited on the landmasses supplying the Cenozoic North Sea basin (the East Shetland Platform was extensive after the Palaeocene uplift), so that smectite remained the main clay product of weathering for a significant period (Pearson, 1990). Alternatively, intrabasinal reworking of lavas or recycling of clays (of volcanic origin) during reworking of exhumed sedimentary rocks may have been contributory. A lack of abrupt changes in the clay mineralogy supplied suggests an homogeneous source area and/or good mixing in the basin (Karlsson *et al.*, 1979). Petrographic evidence provides further tentative evidence for a detrital origin for I-S in Tertiary sediments from Norwegian block 34/10 on the basis of the ragged appearance of flat to undulose platelets under Field Emission Scanning Electron Microscopy (FESEM) (Huggett, 1996).

We suggest that continental soil authigenesis produced the 22/10a-4 smectite before weathering and transport. A detrital, but different source is therefore also most probable for the kaolinite component of the mudstones. Relatively broad kaolinite XRD peaks (mean FWHM 0.38°2θ) noted throughout the lower sequence would also appear to favour a detrital, soil-derived source (Wilson, 1999; Tye *et al.*, 2009). In terms of soil development, kaolinite, along with iron and aluminium oxyhydroxides, is regarded as the typical product of laterites (Ferrosols) and humid, tropical climatic zones such as those found in modern-day Africa, South America and Indonesia (Righi & Meunier, 1995; Bergaya *et al.*, 2006). Significant kaolinite forms throughout the profile as a result of

high rainfall, distributed throughout the year, which produces soil solutions with low concentrations of SiO_2 and basic cations.

Burial authigenesis. As well as debate about whether the clay assemblage initially developed in the marine or continental environment, there is also disagreement over whether the North Sea Tertiary sediments have undergone significant burial authigenesis. The illitization of smectite, or progressive transformation of smectite to illite *via* a series of intermediate mixed-layer I-S species was first recognized in shale diagenetic studies of the Gulf Coast (*e.g.* Hower *et al.*, 1976). Changes in the proportion of illite and smectite and ordering in the I-S have since been correlated and an empirical relationship established with changes in temperature due to burial depth (*e.g.* Pollastro, 1993). These depth-dependent reaction changes in clay minerals have been compared to changes observed in organic materials to construct a Basin Maturity Chart (Merriman & Kemp, 1996). Assuming a 'typical' geothermal gradient of ~25°C/km, the Chart and predominant I-S composition (R0 40% I) suggest maximum burial of ~2.5 km for the 22/10a-4 sequence, similar to the present burial depth. The temperatures and pressures experienced under such shallow burial would be insufficient to alter detritally supplied kaolinite (Merriman & Kemp, 1996). Greater geothermal gradients (40°C/km) and an average reservoir temperature of 107°C for the overlying Forties Sandstone Member suggested by Huggett (1995) cannot have been sustained for a significant period of time. As first highlighted by Ramseyer & Boles (1986), residence time at elevated temperatures is critical in determining the extent of the smectite-to-illite reaction.

Although limited burial transformation of smectite to illite would therefore appear plausible, no direct evidence has previously been provided to the base of the Tertiary (Karlsson *et al.*, 1979; Nielsen *et al.*, 2015). Huggett (1995) also argues that regional, unpublished oil-company XRD data indicate no correlation between I-S composition and depth. However, the marginal, overall increase (30–40%) in illite interlayering in the I-S species with increasing depth through the 22/10a-4 sampled interval, may reflect some limited degree of diagenetic alteration.

Palaeoclimate and palaeohydrology

As stated above, although there are a number of factors affecting clay mineral assemblages (climate, time, parent material, topography, soil-profile type, transport processes, burial diagenesis) (Singer, 1984; Hillier, 1995), palaeoclimate information in the 22/10a-4 sequence is likely to have been preserved as it represents a broad catchment area, is remote from land masses and has undergone relatively shallow burial. By comparison with modern settings, continental soil authigenesis of precursor smectite (I-S) suggests that a seasonal tropical climate with a prolonged dry season was in place during the latest Palaeocene and earliest Eocene in the landmasses surrounding the North Sea Basin. Erratic droughts and floods combined with the dry, deeply cracked vertisol profiles may have led to enhanced erosion and transport to the marine environment (*e.g.* Freebairn *et al.*, 1996).

Increases in kaolinite content in mudstone sequences (frequently evidenced by an increase in the K/S ratio) have often been interpreted to reflect a change to warm and humid conditions and intensified chemical leaching (*e.g.* Robert & Kennett, 1994; Gawenda *et al.*, 1999; Bolle & Adatte, 2001). On this basis, the low K/(I-S) and K/I values recorded in this study (through the Lista Formation and lower Sele Formation Unit 1a, Fig. 8) are interpreted to indicate a seasonal, tropical climate, supplying a smectite-dominated clay mineral assemblage, and increased kaolinite (like the K/(I-S) and K/I 'kicks' and major deflection in the upper Sele Formation Unit 1a) interpreted to indicate a transition to a hot, humid climate. Thiry (2000) argues, however, that the formation of mature, thick kaolinitic soils in equilibrium with the environment requires long-lasting landscape stability of at least 1 Ma. The arrival of soil-clay assemblages in the basin inevitably lags behind their continental formation. John *et al.* (2012) showed, using oxygen isotopes ($\delta^{18}O$), that clays arriving on the New Jersey Margin at the onset of the PETM were most likely to have been reworked from Cretaceous laterites. Therefore, sequential changes in sedimentary clay mineral assemblages with durations of ~1 Ma cannot be caused by climatic changes acting on soil mineralogy, but rather on physical transport processes.

The observed short-term kaolinite anomaly detected in 22/10a-4 is, therefore, more likely to be explained by enhanced fluvial erosion of the pre-existing kaolinite-bearing soils and regolith column rather than chemical weathering and soil formation (*cf.* Schmitz *et al.*, 2001; Foreman *et al.*, 2012; John *et al.*, 2012). Earlier pulses of kaolinite recorded in 22/10a-4 may indicate brief, wetter episodes. These authors argue that a 'kaolinite spike' associated with the PETM reflects an increase in erosion and fluvial discharge, with important implications for hydrology and sediment transport to continental margins.

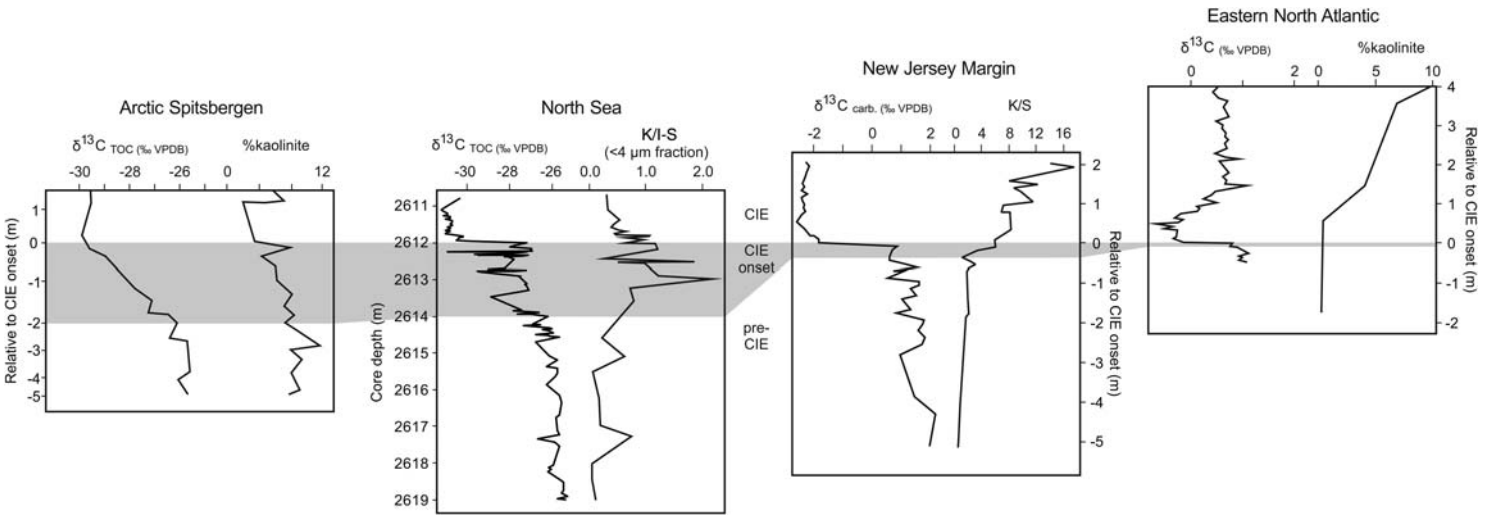

FIG. 9. Comparison of kaolinite (this study) and sediment carbon isotope (from Kender *et al.*, 2012) from 22/10a-4 with recent studies from Arctic Spitsbergen (Harding *et al.*, 2011), New Jersey Margin (John *et al.*, 2012) and the Eastern North Atlantic (Bornemann *et al.*, 2014).

Evidence for such an origin may be provided by the measured crystal order of the kaolinite. The XRD peak widths for the kaolinite-rich samples detected during the CIE onset are significantly sharper (mean FWHM 0.30°2θ) than those lower in the sampled sequence (mean FWHM 0.38°2θ). Such increased crystal order is consistent with erosion and winnowing from lithologies with more advanced diagenetic development, possibly porous sandstones, rather than the more poorly crystalline forms typically produced during soil development (Parry *et al.*, 2015).

Although in some regions the PETM is preceded by a brief (<20 ky) period of aridity (Wing *et al.*, 2005; Kraus & Riggins, 2007; Jaramillo *et al.*, 2010), the PETM is more generally characterized by a humid climate (*e.g.* Robert & Kennett, 1994; Bowen *et al.*, 2004; Adatte *et al.*, 2014) and subsequent hydrological change. Increased sedimentation rates indicate increased precipitation and/or continental erosion, plant- and aquatic-derived biomarker δD compositions indicate increased precipitation and decreased seawater salinity, respectively (Pagani *et al.*, 2006), and surface-water freshening may be indicative of higher river discharge (John *et al.*, 2012; Kender *et al.*, 2012).

Sedimentologically, increased kaolinite in marine sediments is frequently linked with sea-level lowstand deposits as it is typically formed of coarser grain-sizes than other clay minerals, particularly smectite or I-S (Chamley, 1989; Thiry & Jacquin, 1993; Godet *et al.*, 2008; Nielsen *et al.*, 2015). Regional uplift during the late Palaeocene, associated with the proto-Iceland mantle plume, led to a ∼100 m sea-level fall and the observed Lista-Sele facies transition (Knox, 1996). Nielsen *et al.* (2015) interpret increased kaolinite and illite in the margins and increased smectite in the central parts of the North Sea Basin during the Palaeocene as a particle-size sorting effect. However, benthic foraminiferal assemblages reveal that the major kaolinite deposition in New Jersey occurred during times of relatively high sea-levels (Olsson & Wise, 1987; Gibson & Bybell, 1994), suggesting that increased precipitation and erosion was the dominant factor.

Furthermore, evidence for an enhanced hydrological system is presented by the fining-upward particle-size data (this study), palynological, geochemical and sedimentological proxies from the same 22/10a-4 samples (Kender *et al.*, 2012) and North Sea surface-water freshening indicated by shark-tooth apatite $\delta^{18}O$ values (Zacke *et al.*, 2009). An enhanced halocline stratification well before (10^3 y), during the onset, and within the earliest CIE (Fig. 8) may, alternatively, result from the temporary isolation of the North Sea due to a combination of relative sea-level fall, tectonic uplift and basaltic volcanism (Zacke *et al.*, 2009).

Taken together, these results are consistent with an intensification of the hydrological cycle well before the principal carbon release, and the fall of the K/I-S and K/I indices thereafter may reflect the dampening of fluvially derived material as a result of sea-level rise at the principal CIE.

PETM kaolinite distribution

Increased kaolinite concentrations associated with the PETM, as shown in the present study (Fig. 8), have been recorded by many authors from around the world (*e.g.* Robert & Chamley, 1991; Gibson *et al.*, 1993, 2000; Kaiho *et al.*, 1996; Gawenda *et al.*, 1999; Kelly *et al.*, 2005; Soliman *et al.*, 2011; John *et al.*, 2012; Bornemann *et al.*, 2014). However, the precise timing, magnitude and nature of the kaolinite increases is variable with respect to the CIE (Bornemann *et al.*, 2014) (Fig. 9), and non-existent in some regions *e.g.* Bighorn Basin, Wyoming (Gibson *et al.*, 1999). For example, a very significant (∼75%) increase in kaolinite precedes the benthic foraminifera extinction (BFE) by ∼270 ka and the CIE by ∼325 ka in the Zumaia section, Spain (Gawenda *et al.*, 1999). Similarly in Tawanui, New Zealand (Kaiho *et al.*, 1996) the proportion of kaolinite increases just below the CIE, ∼3 ky before the BFE and lasted >∼40 ky. John *et al.* (2012) found a three-fold increase in K/S starting 40 cm below the CIE, peaking 2–3 m above the CIE and returning to pre-CIE values <10 m above the CIE in boreholes from the New Jersey margin (Fig. 9). However, in the Dababiya section, Egypt, a kaolinite spike follows the initial CIE (Soliman *et al.*, 2011). Similarly at the DSDP site 401, eastern North Atlantic, a gradual kaolinite increase, as opposed to a discrete pulse, was identified following the initial CIE (Bornemann *et al.*, 2014) (Fig. 9). A prominent kaolinite spike during the CIE recovery period corresponds with the *A. subsphaerica* acme in the Weddell Sea, near Antarctica, at ODP Site 690 (Kelly *et al.*, 2005). In marked contrast to other studies, kaolinite content declines within the CIE onset in Spitsbergen (Harding *et al.*, 2011) (Fig. 9).

Such variable behaviour in the proportion of kaolinite present in sediments before, during and after the PETM, lends further weight to their origin from increased erosion of soils and/or sedimentary-rock sequences rather than generation by soil-formation processes, as a change to warm and humid conditions might be expected to occur across similar latitudes approximately simultaneously, and

throughout the PETM rather than only in one part of it. In contrast, the variable record in kaolinite content is likely to indicate a combination of: (1) the extent of pre-existing kaolinite deposits; (2) enhanced periods of physical erosion related to intense precipitation (either seasonal or annual changes); and (3) the gradual erosion of available kaolinite. The increases in kaolinite may mark the onset of such precipitation patterns, but subsequent decreases may not signify the termination of intense rainfall if the kaolinite was completely eroded (with no time to form new kaolinite). Overall, the elevation in kaolinite at the PETM noted in this study and in other locations is consistent with an increased hydrological cycle (Pagani *et al.*, 2006) probably taking place immediately before the PETM (Kender *et al.*, 2012). Global variations in PETM kaolinite concentrations are expected, as earth system modelling (Caballero & Langen, 2005) and sediment geochemical studies (Pagani *et al.,* 2006) suggest migrating storm tracks and hydrological cycling with global warming.

CONCLUSIONS

A high-resolution study of clay mineral assemblages from mudstones sampled across the PETM transition and carbon isotope excursion (CIE) onset in North Sea well 22/10-a4 has provided new sedimentological and palaeoclimatic data for this intensively studied sequence. Particle-size data show a marked upwards-fining trend through the sampled sequence, commensurate with an overall eustatic rise. *Newmod-for-Windows*™-modelling of XRD profiles provides improved clay mineral quantification and generally indicates smectite-rich I-S (previously discussed as smectite)-dominated assemblages, the final product of episodes of explosive volcanic activity (Pearson, 1990). It is likely that the smectite-rich I-S formed due to both continental erosion of pedogenic horizons and marine alteration of volcanic ash. I-S development in vertisol soil profiles suggests a prevailing dry, seasonal tropical climate.

Dramatic increases in kaolinite content (~1–50% of the clay assemblage) and K/(I-S) values were detected in the upper part of Sele Formation Unit 1a, prior to the principal CIE but during what now appears to be a complex onset of the PETM, associated with palynological fluctuations (Kender *et al.*, 2012). Previous studies associate such increased kaolinite concentrations in the PETM interval with a change to warm and humid conditions producing intensified chemical leaching. However, the length of time taken to form kaolinite (10^6 years), and isotopic evidence from New Jersey (John *et al.*, 2012), suggest that these were the result of physical weathering of ancient clays by enhanced runoff associated with a more humid climate. The kaolinite anomaly is more likely to be the result of an intensified hydrological regime that caused extensive erosion of pre-existing kaolinite-bearing soils and regolith. Comparisons between the precise timing, magnitude and nature of the kaolinite deviation and other worldwide PETM sequences are consistent with a complex geography of a shifting climate pattern.

ACKNOWLEDGEMENTS

B.G. Group are acknowledged gratefully for allowing access to core samples. The authors thank Jim Riding, Jenny Huggett, Nathalie Fagel, Pierre Pellenard and an anonymous reviewer for their insightful comments which helped improve the manuscript. S.K. was partly supported by NERC Isotope Geosciences Faculty Grant IP/1547/0515. This paper is published with the permission of the Executive Director of the British Geological Survey (NERC). This work was supported by the BGS Climate and Landscape Change research programme.

REFERENCES

Adatte T., Khozyem H., Spangenberg J.E., Samant B. & Keller G. (2014) Response of terrestrial environment to the Paleocene-Eocene Thermal Maximum (PETM), new insights from India and NE Spain. *Rendiconti della Società Geologica Italiana*, **31**, 5–6.

Alt J.C. & Jiang W-T. (1991) Hydrothermally precipitated mixed-layer illite-smectite in recent massive sulfide deposits from the sea floor. *Geology*, **19**, 570–573.

Bergaya F., Theng B.K.G. & Lagaly G. (2006) *Handbook of Clay Science. Developments in Clay Science*, Elsevier, Amsterdam.

Berggren W.A., Alegret L., Aubry M-P., Cramer B.S., Dupuis C., Goolaerts S., Kemt D.V., King C., Knox R. W.O'B., Obaidalla N., Ortiz S., Ouda K.A.K., Abdel-Sabour A., Salem R., Senosy M.M., Soliman M.F. & Soliman A. (2012) The Dababiya Corehole, Upper Nile Valley, Egypt: Preliminary results. *Austrian Journal of Earth Science*, **105**, 161–168.

Berstad S. & Dypvik H. (1982) Sedimentological evolution and natural radioactivity of Tertiary sediments from the Central North Sea. *Journal of Petroleum Geology*, **5**, 77–88.

Biscaye P.E. (1965) Mineralogy and sedimentation of recent deep sea clay in the Atlantic Ocean and adjacent seas and oceans. *Geological Society of America Bulletin*, **76**, 803–832.

Bolle M.P. & Adatte T. (2001) Palaeocene–early Eocene climatic evolution in the Tethyan realm: Clay mineral evidence. *Clay Minerals*, **36**, 249–261.

Bornemann A., Norris R.D., Lyman J.A., D'haenens S., Groeneveld J., Röhl U., Farley K.A. & Speijer R.P. (2014) Persistent environmental change after the Palaeocene–Eocene Thermal Maximum in the eastern North Atlantic. *Earth and Planetary Science Letters*, **394**, 70–81.

Bowen G.J., Beerling D.J., Koch P.L., Zachos J.C., Alroy J. & Quattlebaum T. (2004) A humid climate state during the Palaeocene/Eocene thermal maximum. *Nature*, **432**, 495–499.

Caballero R. & Langen P. (2005) The dynamic range of poleward energy transport in an atmospheric general circulation model. *Geophysical Research Letters*, **32**, doi:10.1029/2004GL021581.

Chamley H. (1989) *Clay Sedimentology.* Springer, Berlin. Heidelberg New York, 623 pp.

Chenot E., Pellenard P., Martinez M., Deconinck J.-F., Amiotte-Suchet P., Thibault N., Bruneau L., Cocquerez T., Laffont R., Puceat E. & Robaszynski F. (2016) Clay mineralogical and geochemical expressions of the "Late Campanian Event" in the Aquitaine and Paris basins (France): Palaeoenvironmental implications. *Palaeogeography, Palaeoclimatology and Palaeoecology*, **447**, 42–52.

Clechenko E.R., Clay Kelly D., Harrington G.J. & Stiles C.A. (2007) Terrestrial records of a regional weathering profile at the Paleocene-Eocene boundary in the Williston Basin of North Dakota. *Geological Society of America Bulletin*, **119**, 429–442.

CO_2.earth. (2016) https://www.co2.earth, accessed on 17/03/2106.

Dypvik H., Riber L., Burca F., Ruther D., Jargvoll D., Nagy J. & Jochmann M. (2011) The Palaeocene–Eocene thermal maximum (PETM) in Svalbard – clay mineral and geochemical signals. *Palaeogeography, Palaeoclimatology and Palaeoecology*, **302**, 156–159.

Foreman B.Z., Heller P.L. & Clementz M.T. (2012) Fluvial response to abrupt global warming at the Palaeocene/Eocene boundary. *Nature*, **491**, 92–95.

Freebairn D.M., Loch R.J. & Silburn D.M. (1996) Soil erosion and soil conservation for vertisols. Pp. 303–362 in: *Vertisols and Technologies for their Management* (N. Ahmad & A. Mermut, editors). Developments in Soil Science, **24**, Elsevier, Amsterdam.

Gawenda P., Winkler W., Schmitz B. & Adatte T. (1999) Climate and bioproductivity control on carbonate turbidite sedimentation (Paleocene to earliest Eocene, Gulf of Biscay, Zumaia, Spain). *Journal of Sedimentary Research*, **69**, 1253–1261.

Gibson T.G. & Bybell L.M. (1994) Sedimentary patterns across the Paleocene–Eocene boundary in the Atlantic and Gulf Coastal Plains of the United States. *Bulletin de la Société Belge de Géologie*, **103**, 237–265.

Gibson T.G., Bybell L.M. & Owens J.P. (1993) Latest Paleocene lithologic and biotic events in neritic deposits of southwestern New Jersey. *Paleoceanography*, **8**, 495–514.

Gibson T.G., Bybell L.M. & Mason D.B. (2000) Stratigraphic and climatic implications of clay mineral changes around the Paleocene/Eocene boundary of the northeastern US margin. *Sedimentary Geology*, **134**, 65–92.

Gillmore G.K., Kjennerud T. & Kyrkjebø R. (2001) The reconstruction and analysis of palaeowater depths: a new approach and test of micropalaeontological approaches in the post rift (Cretaceous to Quaternary) interval of the northern North Sea. Pp. 365–381 in: *Sedimentary Environments Offshore Norway – Palaeozoic to Recent* (O.J. Martinsen & T. Dreyer, editors). Norwegian Petroleum Society (NPF), Trondheim, Special Publication **10**. Elsevier, Amsterdam.

Glennie K.W. (1986) Structural framework and pre-Permian history of the North Sea area. Pp. 26–62 in: *Introduction to the Petroleum Geology of the North Sea* (K.W. Glennie, editor). Blackwell, Oxford, UK.

Godet A., Bodin S., Adatte T. & Föllmi K.B. (2008) Platform-induced clay-mineral fractionation along a northern Tethyan basin-platform transect: implications for the interpretation of Early Cretaceous climate change (Late Hauterivian–Early Aptian). *Cretaceous Research*, **29**, 830–847.

Harding I.C., Charles A.J., Marshall J.E.A., Pälike H., Roberts A.P., Wilson P.A., Jarvis E., Thorne R., Morris E., Moremon R., Pearce R.B. & Akbari S. (2011) Sea-level and salinity fluctuations during the Paleocene–Eocene thermal maximum in Arctic Spitsbergen. *Earth and Planetary Science Letters*, **303**, 97–107.

Harrington G.J. & Kemp S.J. (2001) US Gulf Coast vegetation dynamics during the latest Palaeocene. *Palaeogeography, Palaeoclimatology and Palaeoecology*, **167/1–2**, 1–21.

Harrington G.J., Kemp S.J. & Koch P.L. (2004) Palaeocene–Eocene paratropical floral change in North America: responses to climate change and plant immigration. *Journal of the Geological Society*, London. **161**, 173–184.

Haszeldine R.S. & Russell M.J. (1987) The late Carboniferous northern Atlantic Ocean: implications for hydrocarbon exploration from Britain to the Arctic. Pp. 1163–1175 in: *Petroleum Geology of North West Europe* (J. Brooks & K. Glennie, editors). Graham & Trotman, London.

Hermoso M. & Pellenard P. (2014) Continental weathering and climatic changes inferred from clay mineralogy and paired carbon isotopes across the early to middle Toarcian in the Paris Basin. *Palaeogeography, Palaeoclimatology and Palaeoecology*, **399**, 385–393.

Hillier S. (1995) Erosion, sedimentation and sedimentary origin of clays. Pp. 162–219 in: *Origin and Mineralogy of Clays* (B. Velde, editor). Springer, Berlin, Heidelberg, New York.

Hower J., Eslinger E.V., Hower M.E. & Perry E.A. (1976) Mechanism of burial metamorphism of argillaceous sediments: Mineralogical and chemical evidence. *Geological Society of America Bulletin*, **87**, 725–37.

Huggett J.M. (1992) Petrography, mineralogy and diagenesis of overpressured Tertiary and Late Cretaceous mudrocks from the East Shetland Basin. *Clay Minerals*, **27**, 487–506.

Huggett J.M. (1995) Formation of authigenic illite in Paleocene mudrocks from the Central North Sea: a study by high resolution electron microscopy. *Clays and Clay Minerals*, **43**, 682–692.

Huggett J.M. (1996) Aluminosilicate diagenesis in a Tertiary sandstone-mudrock sequence from the Central North Sea, UK. *Clay Minerals*, **31**, 523–536.

Huggett J.M. & Knox R.W.O'B. (2006) Clay mineralogy of the Tertiary onshore and offshore strata of the British Isles. *Clay Minerals*, **41**, 5–46.

Inoue A. (1995) Formation of clay minerals in hydrothermal environments. Pp. 268–329 in: *Origin and Mineralogy of Clays* (B. Velde, editor). Springer, Berlin, Heidelberg, New York.

Jaramillo C. & 28 others, (2010) Effects of rapid global warming at the Paleocene–Eocene boundary on Neotropical vegetation. *Science*, **330**, 957–961.

John C.M., Bohaty S.M., Zachos J.C., Gibbs S., Brinkhuis H., Sluijs A. & Bralower T. (2008) Impact of the Paleocene–Eocene thermal maximum on continental margins and implications for the carbon cycle in nearshore environments. *Paleoceanography*, **23**, PA2217.

John C.M., Banerjee N.R., Longstaffe F.J., Sica C., Law K.R. & Zachos J.C. (2012) Clay assemblage and oxygen isotopic constraints on the weathering response to the Paleocene–Eocene thermal maximum, east coast of North America. *Geology*, **40**, 591–594.

Kaiho K., Arinobu T., Ishiwatari R., Morgans H.E.G., Okada H., Takeda N., Tazaki K., Zhou G., Yoshimichi K., Matsumoto R., Hirai A., Niitsuma N. & Wada H. (1996) Latest Paleocene benthic foraminiferal extinction and environmental changes at Tawanui, New Zealand. *Paleoceanography*, **11**, 447–465.

Karlsson W., Vollset J., Bjùrlykke K. & Jùrgensen P. (1979) Changes in mineralogical composition of Tertiary sediments from North Sea wells. Pp. 281–289 in: *Proceedings of the 6th International Clay Conference, Oxford, 1978* (M.M. Mortland & V. Farmer, editors). Developments in Sedimentology, **27**, Elsevier, Amsterdam.

Kelly D.C., Zachos J.C., Bralower T.J. & Schellenberg S. A. (2005) Enhanced terrestrial weathering/runoff and surface ocean carbonate production during the recovery stages of the Paleocene–Eocene thermal maximum. *Paleoceanography*, **20**.

Kender S., Stephenson M.H., Riding J.B., Leng M.J., Knox R.W.O'B., Peck V.L., Kendrick C.P., Ellis M.A., Vane C.H. & Jamieson R. (2012) Marine and terrestrial environmental changes in NW Europe preceding carbon release at the Paleocene–Eocene transition. *Earth and Planetary Science Letters*, **353–354**, 108–120.

King C. (2016) *A Revised Correlation of Tertiary Rocks in the British Isles and Adjacent Areas of NW Europe* (A. S. Gale & T.L. Barry, editors). Special reports, **27**. The Geological Society, London.

Kjennerud T. & Gillmore G.K. (2003) Integrated Palaeogene palaeobathymetry of the northern North Sea. *Petroleum Geoscience*, **9**, 125–132.

Kjennerud T. & Sylta S. (2001) Application of quantitative palaeobathymetry in basin modelling. *Petroleum Geoscience*, **7**, 331–341.

Knox R.W.O'B. (1996) Correlation of the early Paleogene in northwest Europe: an overview. Pp. 1–11 in: *Correlation of the Early Paleogene in Northwest Europe* (R.W. O'B. Knox, R.M. Corfield & R.E. Dunay, editors). Special Publications, **101**, Geological Society, London.

Knox R.W.O'B. (1998) The tectonic and volcanic history of the North Atlantic region during the Paleocene–Eocene transition: Implications for NW European and global biotic events. Pp. 91–102 in: *Late Palaeocene-Early Eocene Climatic and Biotic Events in the Marine and Terrestrial Records* (M.-P. Aubry, S.G. Lucas & W.A. Berggren, editors). Columbia University Press, New York.

Knox R.W.O'B. & Morton A.C. (1988) The record of early Tertiary volcanism in sediments of the North Sea Basin. Pp. 407–419 in: *Early Tertiary Volcanism and the Opening of the NE Atlantic* (A.C. Morton & L.M. Parson, editors). Blackwell, Oxford, UK.

Kraus M.J. & Riggins S. (2007) Transient drying during the Paleocene–Eocene Thermal Maximum (PETM): Analysis of paleosols in the Bighorn Basin, Wyoming. *Palaeogeography, Palaeoclimatology and Palaeoecology*, **245**, 444–461.

Lombardi C.J. (2014) Lithostratigraphy and clay mineralogy of Paleocene–Eocene Thermal Maximum sediments at Wilson Lake, NJ. Unpublished MSc Thesis, Rutgers, The State University of New Jersey, USA.

Malm O.A., Bruun Christensen O., Furnes H., Løvlie R., Ruselåtten H. & Lorange Østby K. (1984) The Lower Tertiary Balder Formation: An organogenic and tuffaceous deposit in the North Sea region. Pp. 149–170 in: *Petroleum Geology of the North European Margin* (A.M. Spencer, editor). Norwegian Petroleum Society, Graham & Trotman, London.

McInerney F.A. & Wing S.L. (2011) The Paleocene–Eocene thermal maximum: a perturbation of carbon cycle, climate, and biosphere with implications for the future. *Annual Reviews in Earth and Planetary Science*, **39**, 489–516.

Merriman R.J. & Kemp S.J. (1996) Clay minerals and sedimentary basin maturity. *Mineralogical Society Bulletin*, **111**, 7–8.

Moore D.M. & Reynolds R.C. (1997) *X-ray Diffraction and the Identification and Analysis of Clay Minerals,* 2nd edition, Oxford University Press, New York.

Mudge D.C. (2015) Regional controls on Lower Tertiary sandstone distribution in the North Sea and NE Atlantic margin basins. Pp. 17–42 in: *Tertiary Deep-Marine Reservoirs of the North Sea Region* (T. McKie, P.T.S. Rose, A.J. Hartley, D.W. Jones & T.L. Armstrong, editors). Special Publications, **403**. Geological Society, London.

Murphy B.H., Farley K.A. & Zachos J.C. (2010) An extraterrestrial ^{3}He-based timescale for the Paleocene-Eocene thermal maximum (PETM) from Walvis Ridge, IODP Site 1266. *Geochimica et Cosmochimica Acta*, **74**, 5098–5108.

Nielsen O.B. (1974) Sedimentation and diagenesis of lower Eocene sediments at Ølst, Denmark. *Sedimentary Geology*, **12**, 25–14.

Nielsen O.B., Rasmussen E.S. & Thyberg B.I. (2015) Distribution of clay minerals in the northern North Sea Basin during the Paleogene and Neogene: a result of source-area geology and sorting processes. *Journal of Sedimentary Research*, **85**, 562–581.

Olsson R.K. & Wise Jr, S.W. (1987) Upper Paleocene to middle Eocene depositional sequences and hiatuses in the New Jersey Atlantic Margin. Pp. 99–112 in: *Timing and Depositional History of Eustatic Sequences: Constraints on Seismic Stratigraphy* (C. Ross & D. Haman, editors). Special Publication of the Cushman Foundation on Foraminiferal Research, **24**, Washington, D.C.

Pagani M., Pedentchouk N., Huber M., Sluijs A., Schouten S., Brinkhuis H., Sinninghe D., Jaap S., Dickens G.R. & 302 Expedition Scientists (2006) Arctic hydrology during global warming at the Palaeocene/Eocene thermal maximum. *Nature*, **442**, 671–675.

Parry S.A., Hodson M.E., Kemp S.J. & Oelkers E.H. (2015) The surface area and reactivity of granitic soils: I. Dissolution rates of primary minerals as a function of depth and age deduced from field observations. *Geoderma*, **237–238**, 21–35.

Pearson M.J. (1990) Clay mineral distribution and provenance in Mesozoic and Tertiary mudrocks of the Moray Firth and Northern North Sea. *Clay Minerals*, **25**, 519–541.

Pearson M.J. & Small J.S. (1988) Illite-smectite diagenesis and palaeotemperatures in northern North Sea Quaternary to Mesozoic shale sequences. *Clay Minerals*, **23**, 109–132.

Pollastro R.M. (1993) Considerations and applications of the illite/smectite geothermometer in hydrocarbon-bearing rocks of Miocene to Mississippian age. *Clays and Clay Minerals*, **41**, 119–133.

Ramseyer K. & Boles J.R. (1986) Mixed-layer illite-smectite minerals in Tertiary sandstones and shales, san Joaquin Basin, California. *Clays and Clay Minerals*, **34**, 115–124.

Reynolds R.C. & Reynolds R.C. (1996) *Description of Newmod-for-Windows™. The Calculation of one-Dimensional X-ray Diffraction Patterns of Mixed Layered Clay Minerals.* R.C. Reynolds Jr., 8 Brook Road, Hanover, New Hampshire, USA.

Righi D. & Meunier A. (1995) Origin of clays by rock weathering and soil formation. Pp. 43–161 in: *Origin and Mineralogy of Clays* (B. Velde, editor). Springer, Berlin, Heidelberg, New York.

Robert C. & Kennett J.P. (1994) Antarctic subtropical humid episode at the Paleocene–Eocene boundary – clay mineral evidence. *Geology*, **22**, 211–214.

Röhl U., Westerhold T., Bralower T.J. & Zachos J.C. (2007) On the duration of the Paleocene–Eocene thermal maximum (PETM). *Geochemistry Geophysics Geosystems*, **8**, Q12002.

Schmitz B. & Pujalte V. (2003) Sea-level, humidity, and land-erosion records across the initial Eocene thermal maximum from a continental-marine transect in northern Spain. *Geology*, **31**, 689–692.

Schmitz B. & Pujalte V. (2007) Abrupt increase in seasonal extreme precipitation at the Paleocene–Eocene boundary. *Geology*, **35**, 215–218.

Schmitz B., Pujalte V. & Nunez-Betelu K. (2001) Climate and sea-level perturbations during the initial Eocene thermal maximum: evidence from siliciclastic units in the Basque Basin (Ermua, Zumaia and Trabakua Pass), northern Spain. *Palaeogeography, Palaeoclimatology, Palaeoecology* **165**, 299–320.

Schultz L.G. (1964) Quantitative interpretation of mineralogical composition from X-ray and chemical data for the Pierre Shale. *U.S. Geological Survey Professional Paper* 391-C, 31 pp.

Shepard F.P. (1954) Nomenclature based on sand-silt-clay ratios. *Journal of Sedimentary Petrology*, **24**, 151–158.

Singer A. (1984) The palaeoclimatic interpretation of clay minerals in sediments – a review. *Earth Science Review*, **21**, 251–293.

Sluijs A., Brinkhuis H., Schouten S., Bohaty S.M., John C. M., Zachos J.C., Reichart G., Sinninghe Damste J.S., Crouch E.M. & Dickens G.R. (2007) Environmental precursors to rapid light carbon injection at the Palaeocene/Eocene boundary. *Nature*, **450**, 1218–1221.

Sluijs A., Brinkhuis H., Crouch E.M., John C.M., Handley L., Munsterman D., Bohaty S.M., Zachos J. C., Reichart G., Schouten S., Pancost R.D., Sinninghe Damsté J., Welters N.L.D., Lotter A.F. & Dickens G.R. (2008) Eustatic variations during the Palaeocene–Eocene greenhouse world. *Paleoceanography*, **23**.

Soliman M., Aubry M.-P., Schmitz B. & Sherrell R.M. (2011) Enhanced coastal productivity and nutrient supply in Upper Egypt (PETM) during the Paleocene/Eocene Thermal Maximum: Mineralogical and geochemical

evidence. *Palaeogeography, Palaeoclimatology, Palaeoecology*, **310**, 365–377.

Thiry M. (2000) Palaeoclimatic interpretation of clay minerals in marine deposits: an outlook from the continental origin. *Earth-Science Reviews*, **49**, 201–221.

Thiry M. & Jacquin T. (1993) Clay mineral distribution related to rift activity, sea-level changes and palaeo-oceanography in the Cretaceous of the Atlantic Ocean. *Clay Minerals*, **28**, 61–84.

Tripati A. & Elderfield H. (2005) Deep-Sea temperature and circulation changes at the Paleocene–Eocene thermal maximum. *Science*, **308**, 1894–1898.

Tye A.M., Kemp S.J. & Poulton P.R. (2009) Responses of soil clay mineralogy in the Rothamsted classical experiments in relation to management practice and changing land use. *Geoderma*, **153**, 136–146.

Wentworth C.K. (1922) A scale of grade and class terms for clastic sediments. *The Journal of Geology*, **30**, 377–392.

White A.F. & Brantley S.L. (1995) Chemical weathering rates of silicate minerals; an overview. Pp. 1–22 in: *Chemical Weathering of Silicate Minerals* (A.F. White and S.F. Brantley, editors). Reviews in Mineralogy and Geochemistry, **31**, Mineralogical Society of America, Washington, D.C.

Wilson M.J. (1999) The origin and formation of clay minerals in soils: past, present and future perspectives. *Clay Minerals*, **34**, 7–25.

Wing S.L., Harrington G.J., Smith F.A., Bloch J.I., Boyer D.M. & Freeman K.H. (2005) Transient floral change and rapid global warming at the Paleocene–Eocene boundary. *Science*, **310**, 993–996.

Zachos J.C., Wara M.W., Bohaty S., Delaney M.L., Petrizzo M.R., Brill A., Bralower T.J. & Premoli-Silva I. (2003) A transient rise in tropical sea surface temperature during the Paleocene–Eocene thermal maximum. *Science*, **302**, 1551–1554.

Zacke A., Voigt S., Joachimski M.M., Gale A.S., Ward D. J. & Tütken T. (2009) Surface-water freshening and high-latitude river discharge in the Eocene North Sea. *Journal of the Geological Society, London*, **166**, 969–980.

Zeelmaekers E., McCarty D. & Mystkowski K. (2007) *SYBILLA User Manual.* Chevron proprietary software, unpublished manual, Houston, Texas, USA, 16pp.

Zeelmaekers E., Honty M., Derkowski A., Środoń J., De Craen M., Vandenberghe N., Adriaens R., Ufer K. & Wouters L. (2015) Qualitative and quantitative mineralogical composition of the Rupelian Boom Clay in Belgium. *Clay Minerals*, **50**, 249–272.

Ziegler P.A. (1982) *Geological Atlas of Western and Central Europe.* 130 pp. + folder with 40 maps or charts.: Shell Internationale Petroleum Maatschappij B.V., The Hague; Elsevier Scientific Publishing Company, Amsterdam, The Netherlands.